

## **Wilkinson Power Divider for High Power Amplifier Employed for Wireless Communications**

**Suham A. Albderi**

Al-Furat Al-Awsat Technical University, 31003, Najaf, Iraq

*Received 4<sup>th</sup> Oct 2023, Accepted 6<sup>th</sup> Nov 2023, Online 6<sup>th</sup> Dec 2023*

**Abstract:** High power amplifier based on the Wilkinson energy has been constructed and fabricated in this study. The 45-50W primary speaker unit is manufactured using horizontally distributed metal oxide semiconductor (LDMOS) materials and ferromagnetic materials. Field Effect Transistor (FET) Transistor PTFA260451E. Wilkinson Energy Complex has employed to merge dual entered energies to achieve 90 watts of power. The suggested power amplifier was investigated, planned and advanced utilizing (MATLAB) software traditional Wilkinson power dividers (WPDs) might produce acceptable response near to suggested center frequency Anyhow, such WPDs might further displayed low out of range response whereas it needs adding significant procedures. In favor of enhancing the preset performance state, a modification has been made Proposed utilizing microstrip WPD which shows significantly improved stopping range with large separation. A low-pass filter (LPF) model is employed in each sections of the harmonic damping splitter to save power. The suggested structure is constructed using microelectromechanical system oscillators (MEMS) against the film's sonic resonator (FBAR) with a center frequency of 2.65-3 GHz with two sections and 50 Ohm impedance for 90 watts amplification power.

**Keywords:** Wilkinson Power Dividers (WPDs), High Power Amplifier, Field Effect Transistor (FET), Low-Pass Filter (LPF), MATLAB Software, Wireless Communications.

### **1. INTRODUCTION**

Part of the essential and indispensable equipment in radio communications systems is the power amplifier (PA), primarily in lengthy separation communication structures such as mobile as well as satellite communications. Power amplifiers amplify the RF waveform for antenna driving and produce the most capable gain minimum available reflection. Many studies have appeared on the design and manufacture of power amplifiers that operate in various spectrum ranges also evaluate problems such as: advancing energy against efficiency ascending the circuit spectrum band also reducing the distraction in the intermodulation [1-10]. Newly, various techniques to construct huge energy with frequency range, PAs have been investigated and suggested. Part of the utmost utilized investigation oversights is to be based on a multi-stage power amplifier system [11-15]. Anyhow, this approach has little reliability, due to that, whenever a section of the power amplifiers folds, the model will not activated. Another investigation oversights are studied as well proposed, such that, the constructions are based on parallel power amplifier against power divider/mixer [16-20]. Thus, this study focuses on advancing the amplifier power utilizing

a wilkinson power divider/mixer using a broad spectral range. In order to employ such thing, two low-power amplifiers with narrowband spectrum are constructed also mixed utilizing the power merger. Figure 1 presents the power amplifier general schematic chart[12-20].

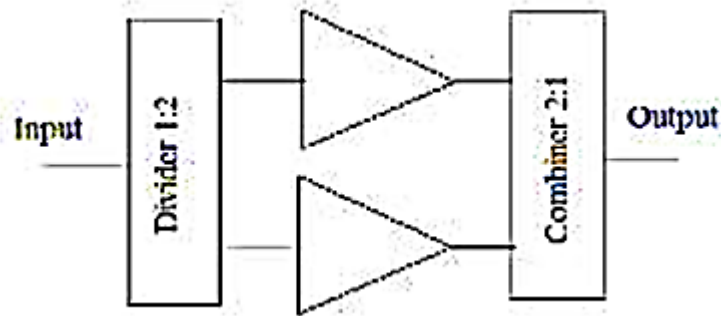


**Figure 1: General block diagram of the power amplifier [12-20].**

Microstrip filters such as band-pass filters (BPFs) with low-pass filters (LPFs) show a dominant role in the construction.

MEMS based resonators have arisen as an alluring elective that might offer Q-values near which for quartz in both vacuum just as in air also projecting recurrences up to the extremely high recurrence (VHF, 30 MHz-300 MHz) also super high recurrence (UHF, 300 MHz-3 GHz) values, expand minimum energy, give heat strength best than 18 ppm north of 27 to 107°C with maturing soundness better than 2 ppm north of one year, have more limited plan with creation process durations, as well as might be monolithically integrated as well as fabricated utilizing minimal expense CMOS viable cycles [13-18]. Furthermore, MEMS resonators are exceptionally vigorous to stun as well as vibration, as well as provide a mind-boggling extent advantage. In any case, for substitution of the quartz precious stone innovation with MEMS, the last option requires to effectively defeat a couple of issues connected with heat dependability, warm hysteresis, long haul soundness, bundling as well as so upon These issues are step by step being addressed, also the circumstance also recurrence control industry have begun accepting the MEMS resonator based gadgets [4].

Both capacitive [15,16] against piezoelectrical transduced [17,18] renditions of micromechanical resonators have been illustrated. Different applications enveloping such resonators, including RF sifting with blending have likewise been accounted [19]. Some earlier studies upon MEMS resonators are accessible in the writing. A phenomenal audit by Nguyen [20] zeroed in upon the different parts of RF MEMS resonators, channels, as well as reference oscillators. Silicon micro-machined resonators have likewise been assessed in the study upon RF MEMS innovation by Kim as well as Chun [21]. Lam [22] suggested a complete audit of MEMS as well as quartz gem innovations utilized in recurrence control implementations according to a modern viewpoint. This study expands regarding the matter by exploring the most recent turns of events, while at the same time giving an orderly record of the various calculations, vibration modes, mechanical as well as electrical comparable models, creating materials, as well as RF utilizations of such resonators; as well as consequently might fill in as an instructional exercise for small extent electromechanical resonators field.

MEMS resonators which are capacitively transduced are overall inclined into their piezoelectrically transduced partners. Additionally among the previous assortment of micro-resonators, mass acoustic mode of vibration is the favored choice for acknowledging huge recurrence of activity [23]. Along these lines, other than a depiction of the different revealed MEMS resonator types also forms of fluctuation, such audit provides a committed spotlight upon the activity also modeling of a circle resonator which has a place with the specific assortment of mass form resonator in light of capacitive transduction. And yet,

this does the trick for realizing of the standard behind flexural-mode resonators too. The strategies as well as materials utilized by different exploration bunches for manufacture of MEMS resonators have additionally been explained against the comparing benefits also detriments. The misfortune components liable for dispersal of such resonators vibration power which have additionally been examined. Light has additionally focused upon a portion of the revealed utilizations of RF MEMS full gadgets, similar to oscillators also channels. Moreover, the possibilities of combination of MEMS actuators and sensors against CMOS hardware have been momentarily explored. At long last, a few future exploration headings have been given which ought to empower the joining of such resonators into the mainstream of electronic specialized gadgets. Figure 2 illustrates a typical samples of the MEMS FBAR actuators [24,25].

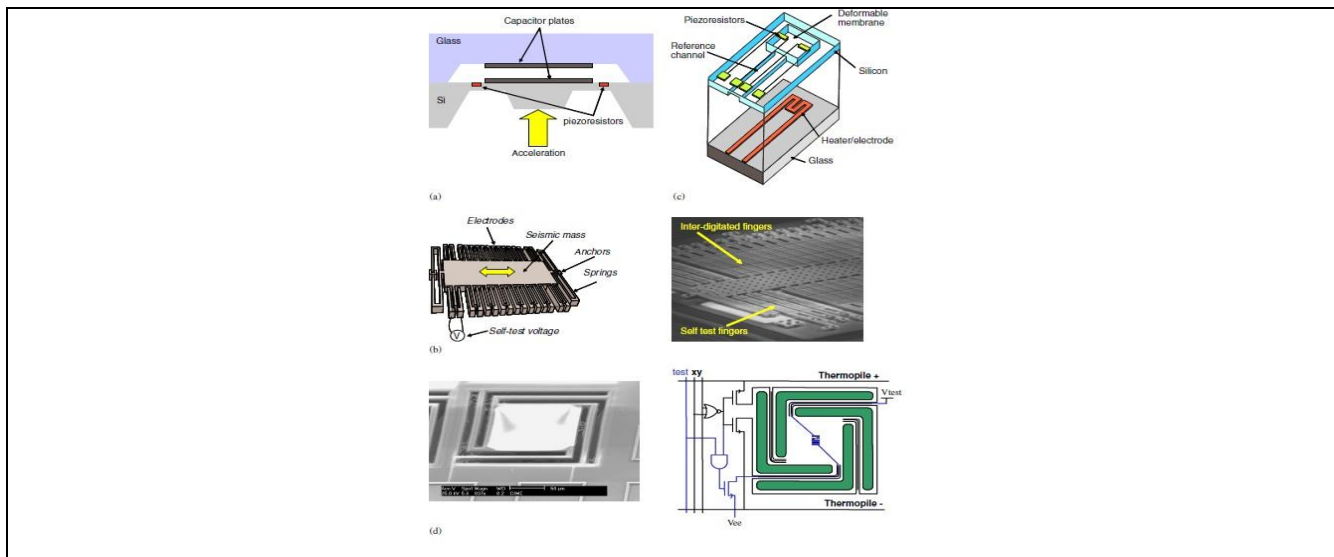


Figure 2: Typical samples of the MEMS FBAR actuators [15-18].

## 2. RELATED STUDIES

A portion of the important articles discussing the behavior of electromechanical resonators and power amplifiers has been collected and reviewed in the following paragraphs: The fundamental properties of mechanical resonators are important and effective factors which cannot be completely settled by the resonant spectrum and attribute component (power distraction). At the normal spectrum of any ideal mechine-driven vibration building, the animated force of a given automated fluctuation is equivalent to the inherent force saved in the comparative resonance deformity of the building. Therefore, when self-frequency is achieved, the overall power in the automated frame is forever moved in this way with the average kinetic force being applied in addition to the inherent power. Anyhow, a true mechine-driven construction would suffer power cost at every oscillation phase. In a true automated construction against changing force magnitudes, the eigenmode component is named vibration echo or resonance. The concept of repetition to equip energy as well as potential energy amid the kinetic force is called resonance repetition, that is generally near to the characteristic repetition of a similar frame [5]. Lee et al. Two excellent metal-film nanocantilever operating at very high frequencies were fabricated as described in [8]. The length of the cantilever is 600 nm - 30  $\mu$ m, and its width is greater than 400 nm - 5  $\mu$ m. With dual tied stages that backing it as an electrifying means, in addition to the capacitor for pressure. All cantilever beams are ultra-fabricated from a single 70nm thick SiC precious stone and are additionally protected by a metal covering. By reducing the resonant range, the resonant spectrum continues to expand. At the point where the resonant amplitude diminishes to 0.6 \* 0.4 \* 0.1  $\mu$ m, the resonant frequency reaches 127 MHz [10]. Thus, in order to obtain greater super-repeatability, Huang et al. manufactured double-entangled resonant oscillators formed from 3C-SiC film with a huge echo resonance recurrence of 1.029 GHz,

making the nano-electro-mechanical system (NEMS) resonant oscillators reach the microwave radiation area [12]. As the thickness of the vibrating pattern decreases, the basic stress of the starting substantial has an increasingly greater effect on the resonator mechanical settings. The bulk of the very slight resonances emerge in the overstressed area, presenting a robust credence on the viewpoint ratio  $L/t$ . In order to make dominant-mode resonant oscillators, Zhou et al. Offering an rabid-slim, huge-visibility rate by proposing a double-lattice nano-mechanical resonator with an  $L$  length of up to  $111\mu\text{m}$ , a thickness as low as  $22\text{nm}$ , and, moreover, with a visibility ratio of up to  $L/T \sim 5000$ . Less pressure eith an inner axis of  $6.3^*$  in Figure 10-8, where the different vibration modes of the motion resonance frequency at lounge heat generally meets the Euler-Bernoulli column hypothesis expected value. In order to access the nanomechanical resonant oscillators stress-free cutting, unaided  $\text{Al}_2\text{O}_3$  ribbons composed by atomic layer deposition (ALD) are relocated into the pre-sculpted channels. Throughout the exchange cycle, the inherent pressure generated by the collecting system is delivered, production in resonance accumulation against extremely little pressure [13]. Hence, in general, accepted that huge awareness needs good elements, with the prime location (also high awareness) is influenced by two elements: limited line width and noise signal. Since it is not completely settled by the resonator quality variable, the latter option is also evaluated by calculating the signal-to-noise rate. Whatever the case, Roy et al. using the idea in which repetitive oscillation disturbance relates to the quality component below low data transmission without using high  $Q$  estimation plus a huge absorbing model against complete unique access must produce improved repetitive power (as well as awareness) than a similarly low damped range. Concerning the confirmation of such theory, a nano-optical mechanical framework (NOMS) has been utilized, such that a double-cut shaft is dual to a racetrack optical hole resonator as well as identified by a tunable diode laser. Along the thermal interaction of the resonator, the thermal target of  $60\mu\text{K}$  is obtained at  $300\text{Hz}$  data transmission power, that gives a new idea to use ultra-precision resonators for elite implementation in gas or liquid atmosphere [17]. The resonator nonlinearity might be based on merging among bound areas or middle-level expanding. The after-effect of non-linear impacts is to compose the resonator occure bi-stationary, have loose or pinned behaviour, chaotic, etc. To simplify the construction with also explaine the nonlinear productives better, Taja Dediyan-Far et al. With proposals that specify the homogeneous analysis method (HAM) in the scientific arrangement of the resonator interaction, and as the article showed that the second arrangement is utilized via the assignable limits, which assumes an important role in projecting on the scientific expression efficiency of the nonlinear obstacle unambiguously. Due to this scientific arrangement, it has been suggested to perform stabilization, relaxation, or mixing practices close to the fundamental resonant frequency [16]. Jin et al. They schemed a robust nonlinear model given the fundamental photon-electron bonding as well as the energy band hypothesis to depict etch-free opto-automated merging. Along the virtual scheme, the laser energy might be adjusted and the recurrency might be controlled to create the effect of conditioning and anchoring the resonator for increased control. In addition, the unique reaction of the nano-electro-mechanical system (NEMS) resonator, which has different dendrites, can be obtained through the use of parametric laser dynamic. It is observed that the turbulent state might being composed at a few apparent recurrences of the filled laser. The employ of lasers to control the nanoresonator provides an incentive to study its nonlinear implementation [11]. Also, vibrational coupling is strengthened in a resonator with carbon nanotube, ahainst the amplitude minimized to the subatomic leveled, there is strong connectivity, and surprisingly weak warm variations might make the oscillator appear nonlinear [14]. The the piezoelectric effect are utilized by Masmanidis et al. to construct a resonator called NEMS. An AC signal is utilized for resonator driving, using a DC voltage which employed to change the width of the depletion region. The crossed electric field produces longitudinal stress in the cantilever beam, and a bending second is generated due to asymmetric stress allocation compared to the non-partisan axis of the beam resulting in mechanical resonance. Since the strain drive occurs mainly in the high-resistance depletion region, the width of the depletion region may be changed by changing the AC voltage, and in this way the piezoelectric throughput is adjusted to

change the permittivity of the resonator. At the same time, a two-slit cantilever beam is generated, which may be related with a DC standby to adjust the resonance frequency as shown in [20]. To address the issue of moderate development coefficient intersection, Guzman et al. proposes to involve silicon carbide (SiC) as the resonant element. Also free for frequency equalization to accomplish frequency tuning [22]. For cantilever beams with rigid and attractive electrical connections as well, the piezoelectric voltage generated by the strain upgrades the multi-iron signal transmission. HDC is used for resounding frequency tuning. Due to ME coupling, the piezoelectric signal also changes with the full frequency variation [23]. Jia et al. They searched for most micromechanical resonators with a bending scheme applied in fluids. The micro-disc resonator is made of silicon carbide and also features multi-mode resonance in air and water. Up to 28 curvature patterns were observed in air with 12 in water, with frequency ranges from ~3 to 190 MHz with Qs up to ~30 [25]. The quality component determines the rate at which the nanomechanical resonator consumes energy. Methods of energy dissipation include loss of contact with the surrounding liquid or gas medium, loss of elastic wave reinforcement generated to the substrate, or again intrinsic use of the resonator, for example, loss of thermoelasticity. Scatterplot. The vast majority of micromechanical resonators require excellent parameter realizations to be applied [26]. To focus on the quality component of the resonator as well as reduce the power loss, Aykol et al. The fabricated suspended carbon nanotubes are placed over metal cathodes and their resonance properties are stabilized by weak van der Waals forces. Since the cutting conditions remain unchanged, regardless of whether the temperature is increased or not, the nanotubes are isolated along the sidewalls and do not affect the quality component. [59]. Another huge loss to the resonator comes with the effective liquid climate. When the resonator resonates in the liquid, more massive energy loss occurs due to dense damping. Fairbridge et al. They presented the fabrication of single and double-stabilized SiN nanoresonators as well as their placement in air, alcoholic beverages and water as well as a cushion for resonance [27]. To obtain a double clamp beam with a length of 2  $\mu\text{m}$ , a width of 165 nm and a thickness of 125 also adjust the voltage of the scheme, the adequacy and the frequency of the resonator as well. (a) Mode separation occurs when the door voltage changes. Modified by license at length [28]. (b) The resonance amplitude depends on the difference in AC voltage. Edited for length [29]. (c) Constant AC voltage, and the frequency depends on the difference in DC voltage. Modified with license at length [30].

### 3. METHODOLOGY

For advanced communications models whereas they are utilized to discard unwanted waveforms and harmonics along radio waves. The BPF filter is a little volume, less insertio loss (IL) constructed utilizing linear coupled resonator oscillators with a parody outside plasmon resonator oscillators have been presented for communications implementatios. Furthermore, BPFs participate an importat aspect in demodulating or receivig either relevant waveforms along a modulated wave in modern remote communications circuits and RF waveform receivers [14-22]. The Geisel power divider with the Wilkinson power divider (WPD) are very mutual as well as useful power dividers. In RF/microwave communications circuits to split an entered waveform towards two output waveforms which are in phase, or to mixing two equal-phase waves towards a mixed waveform using a 180 degree phase shift. Relied on the swift advancement using the latest communications, the need for multiple-bandwidth spectrum parameters has advanced seriously in the last years. Anyhow, traditional WPDs have a huge area which require a little blocking bandwidth. Extra measures such as double-linearization and mixed filters mitigate such obstacles. Along past researches, a broadband BPF power divider against attenuation technique utilizing microstrip seed with coupled lines was introduced [20-26]. A short time ago, many approaches have developed such as microstrip seed, electromagnetic bandgap microstrip componets, bent heel and rectangular resonator, asymmetric spiral DGS, huge using little impedance resonators, SMD inductors and resistors. The seed is radially open they were employed to construct harmonic suppression models. In advanced communications models, the need for multiplexer and multiport components e.g., as power

splitters and diodes grow rapidly. Furthermore, the construction of LPF, BPF and adjustable microchip apparatus relied on LC circuits with analytical approaches might further be very useful. Moreover, every LPF with BPF components like ROR, SF, NORMALIZED Circle Size (NCS), Figure of Merit (FOM), Relative Stop Band (RSB), as well as the tuning range (TR), cut-off frequency (fc) with center frequency (f0) were investigated [22-28]. A power divider is an apparatus utilized to split entered energy toward multiple achieved energy depending to costruction demands using energy harvesting to merge multiple entered energies toward resulting energy. Along experimentation, a planner might utilize several various kinds of dividers such as directional couplers, also T-junctions the two lines with Wilkinson dividers. The T-junction power splitter is the elemental, a 3-port network utilizing single entrance along dual exits. Anyhow, part of the drawbacks of such circuit is poor insulation amidst the results multiple. To evaluate such obstacle, a Wilkinson power divider (WPD) will be employed in such investigation. In a Winkinson power divider amplifier model that is inserted among the output ports a high isolation capacity will be constructed such that, the WPD part is preseted in Figure 3 [14-23].

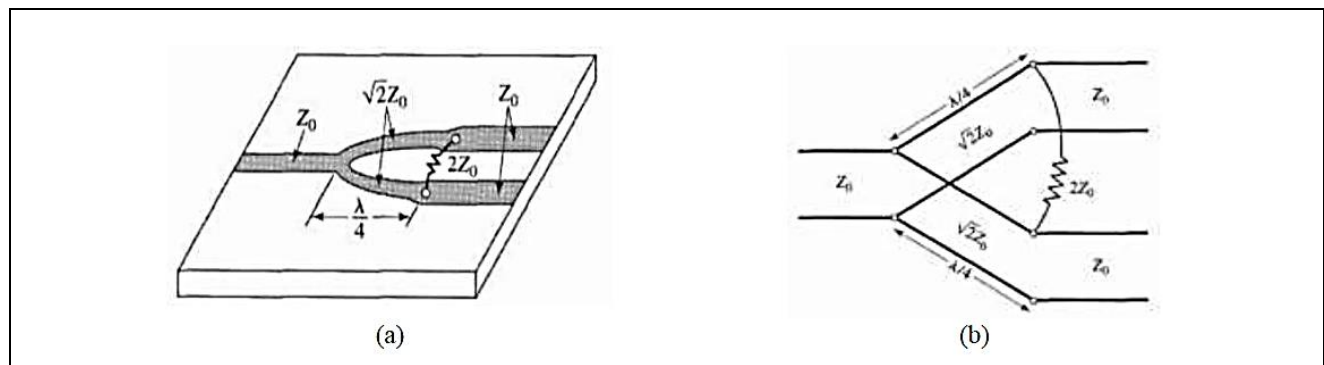


**Figure 3: The WPD part, (a) Micro-trip form of Wilkinson power divider, (b) Equivalent transmission line Circuit [14-23].**

The two-way Wilkinson power divider employes a quarter-wavelength line ( $\lambda/4$ ) to equalize the  $Z_0$  entered impedance with  $2 \cdot Z_0$  resistance attachig the outcome, such that the cross-section resistance is  $\pi/4$ . So  $Z_0/4 = \sqrt{2} \cdot Z_0$ , that composes such splitter obtain narrow range. For realizing a large-scale splitter/collector, a multi-section impedance matching approach having  $\pi/4$  sections at 2.65 GHz center frequency is suggested in this study. The sections amount was sellected as 2,  $Z_0 = 50 \Omega$ , with  $Z_L = 100 \Omega$ . Table 1 illustrates the evaluatios results of WPD resistance properties.

**Table 1: WPD resistance evaluatios results properties [15-24].**

Sections Number	$Z_0$ (Ohm)	$Z_1$ (Ohm)	$Z_2$ (Ohm)
2	50	84	60

To design a 50W power amplifier, the convenient transistor PTFA260451E was selected. The transistor produced by infineon techniques is used as a model in such study. It is a high power thermally improved LDMOS FET transistor against an output power of 50 watts and activates at a central frequency of 2.65 GHz. The power amplifier has been constructed along the incoming steps: First, the stability of the transistor should be checked utilizing the transistor s parameter. Second: It should be stable within the required frequency range. The utilize of parameters K with  $\Delta$  is part of the necessary criteria for determining the stability of a power amplifier (PA) client [14-23].

$$K = 1 - \frac{|S_{11}|^2 - |S_{22}|^2 + |S_{11}S_{22} - S_{12}S_{21}|^2}{2|S_{12}S_{21}|} \quad (1)$$

$$\Delta = S_{11}S_{22} - S_{12}S_{21} \quad (2)$$

PA activates using unconditional stability if  $K > 1$  and  $|\Delta| < 1$ . On the second aspect, relied on the dispersion coefficient of the transistor, and in order to construct the input and output impedances to be transistor matching with source and load impedance. Several plan techniques were tried impedance matching such as utilizing summed elements; microstrip line such as unique heel or double heel. Anyhow, such approaches provide a arrow impedance matching. Thus, in order to obtain high power with broadband impedance matching with stability, such planning suggests the employ of multi-section transformers. The suggested structure is constructed with a center frequency of 2.65-3 GHz, and contains of input resistance matching, output matching.

The procedur utilized for applying the suggested MEMS self test model has been approved after reviewing similar previous projects as well as investigating the available literature, depending upon the objectives of this study. In this study, the planned structure proposed for robust as well as efficient monitoring as well as controlling design for micro-electromechanical resonator structure is illustrated in Figure 4.

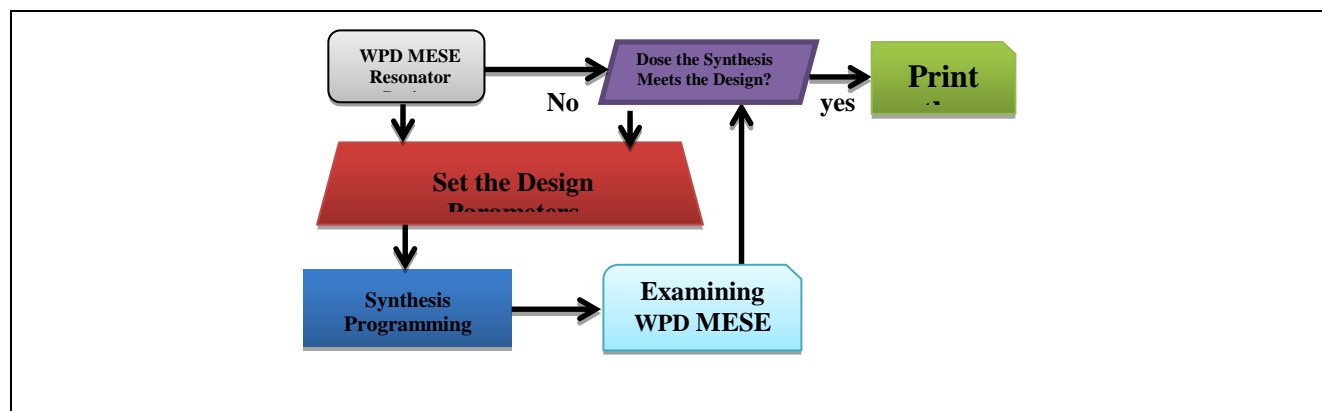


**Figure 4: The designed robust micro-electromechanical WPD-MEMS resonator structure.**

The idia of the self test proposed model actuator is summarized by refeering to the model shown in Figure 4, such that the WPD-MEMS resonator will set the design according to the physical parameters specifications of the piezoelectrical materials provided by the synthesized programming block. The resulting WPD-MEMS designed parameters will be examined through the examining MEMS block and then the outcomes will be compared with the actual results produced along the original MEMS resonator blok. Finally, if the comparison results are not be matched, the design set procedudre will be repeated, else, the results will be printed. In order to implement the proposed model, a MatLab2021b simulation program has been applied with Simulink tool box utilities.

Presently, the hypothetical and commonsense subtleties that have employed to construct the suggested resonant filter would be explained by picking the suitable piezoelectric substaintials as far as (material sort, aspects, thickness, wave and transmission speed). Subsequent to deciding the details of the piezoelectric substaintials employed to plan the resonant filter (FBAR), the supported numerical relations will be expressed to address the filtering component. Along implementing such relations, each quality of the resonant filter, such as, the impedance and frequencies will be achieved. In reality, notwithstanding the FBAR band pass filter plan equations examined in the past segment Equations (3) to (6), the upsides of the pause and pass band pass filter frequencies,  $f_s$  and  $f_p$  with the BPF quality variable,  $Q$ , might be tracked down along one further supporting modeling equations as following :

$$\epsilon = \frac{Z_{Acoustic}}{V \times D} \quad (3)$$

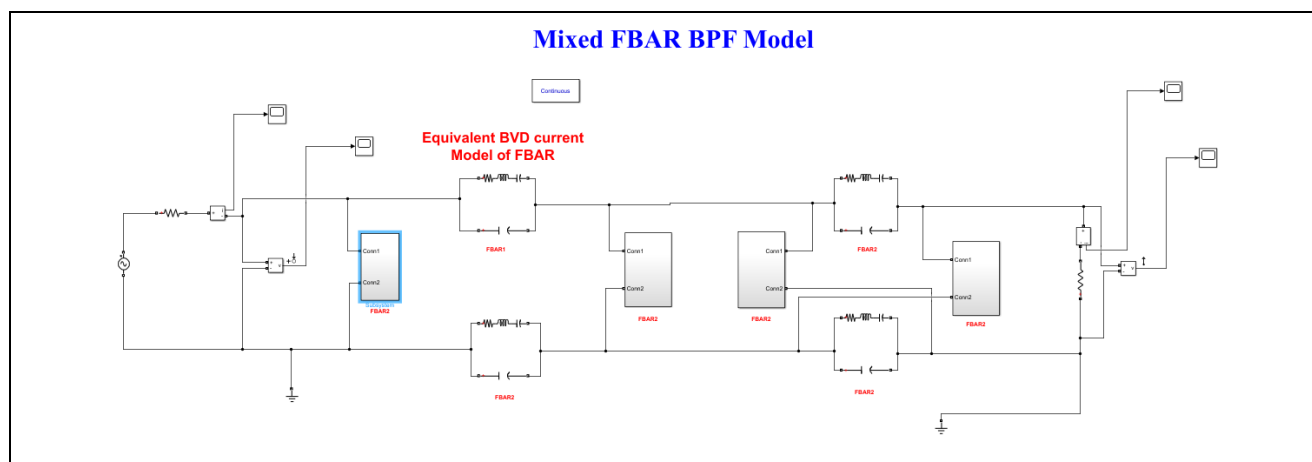
$$f_p = \frac{V}{h} \tag{4}$$

$$f_s = 0.85f_p \tag{5}$$

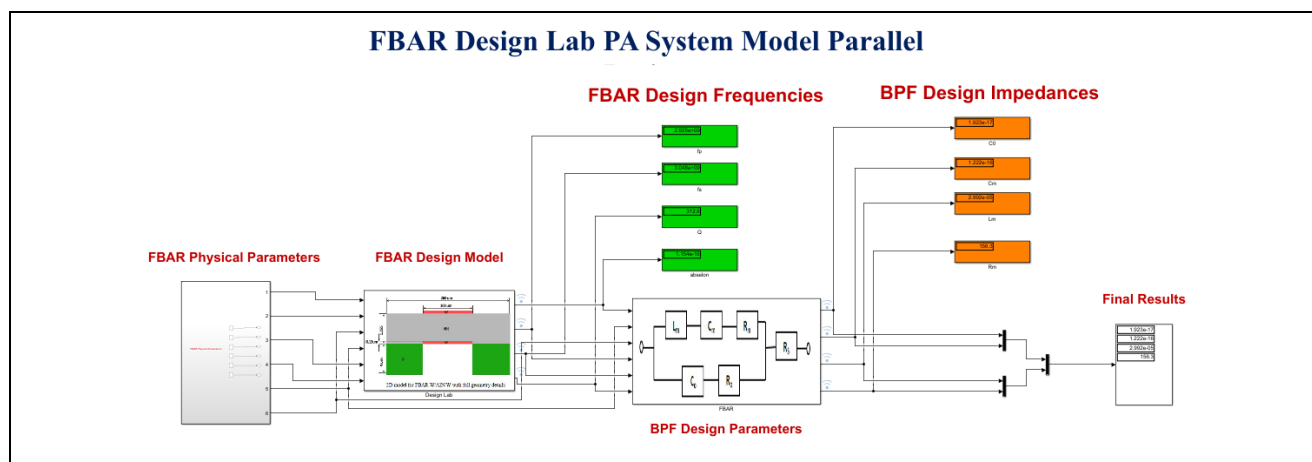
$$Q = \frac{f_s \times d}{0.05 \times f_p \times A} \tag{6}$$

In which,  $Z_{Achoustic}$ , is the FBAR acoustic impedance,  $V$ , is the FBAR acoustic speed,  $D$ , is the piezoelectric material thickness, and  $d$  is the slim film FBAR thickness deviation. As it is obvious along the past equations, the actual boundaries of the FBAR dainty - film substantial will conclude the band-pass filter plan upsides. The above relations will find the expected FNAR plan boundaries accepting fixed DC biasing upsides of 25 V and around straight examination , The suggested plan lab framework scheme will mimic such relations involving the MatLab2022a Simulink tool compartment for design the necessary FBAR band-pass filter plan boundaries values.

Figure 5 presents the costruction details of the FBAR DC bias with DC power is given via a quarter-signal communication line so this does not exist to disturbed against AC waves.



(a)



(b)

**Figure 5: The costruction details of the FBAR DC bias with DC power is given via a quarter-signal communication line so this does not exist to disturbed against AC waves, (a) WPD model with FBAR mixed construction, (b) WPD internal parameters desig modelling .**

As shown in Figure 5, the power amplifier is represented by the equivalent circuit of the Film Bulk Acoustic Resonator chip (FBAR), which are represented as BPF filters, are connected in the mixture method, and they are represented utilizing the MATLAB program software as presented in Figure 5.a. Figure 5.b, also presets a representation of the Wilkinson power amplifier represented by simulating the physical variables which construct the material of such amplifier chip, those are controlled through equivalent mathematical equations which describe the relationships among such variables to find the working frequencies and the spectrum band of the filter that represents the characteristics of such amplifier..

By modifying the design of the WPD-MEMS filter a parallel frequency of  $f_p$  of 3 GHz with a quality factor  $Q$ , 850 will be achieved. Table 2 shows the construction components employed in the planning software with the achieved parameters of the WPD-FBAR filter obtained for cut-off frequency  $f_c=2.65\sim 3\text{GHz}$ .

**Table 2: WPD-FBAR filter resulting design parameters employed in the program for  $f_c=3\text{ GHz}$ .**

FBAR Componets	V Acoustic Speed (m/s)	h PA thickness (m)	d PA thickness deviations (m)	PA area ( $\text{m}^2$ )	Acoustic Impedance $Z_{\text{achoustic}}$ (Ohm)	PA Density ( $\text{Kg}/\text{m}^2$ )
	3e6	1.1e-6	2.1e-3	4.05e-4	9.98	0.975e7
$f_p$ (Hz)	3e9					
$f_s$ (Hz)	2.65e9					

#### 4. RESULTS OF SIMULATION

The suggested models presented in Figures 4 and 5 were successfully designed, simulated, and implemented with the designed specifications shown in Tables 1 and 2. The designed frequency variation ratio was adjusted from 0-50%, and successfully simulated, with the switching values of the MEMS power amplifier frequencies generated by the self-test. The suggested WPD-MEMS model has been implemented utilizing MATLAB tool box with m. files script codes according to the specefied design parameters and constraints. The results of the employed suggested WPD-MEMS model have been shown as illustrated in Figure 6 for the obtained time signals.

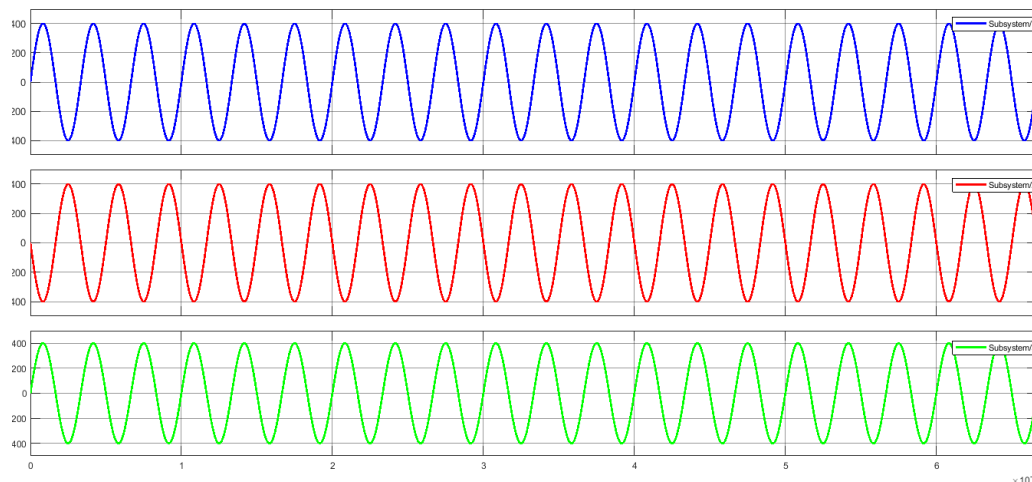


**Figure 6:** Results of the implemented WPD-MEMS model in time domain.

As presented in Figure 6, we could observe the sinusoidal signals in time domain employed to examine the suggested WPD-MEMS model. The blue color sinusoidal signal is the entered activated test signal with 3 GHz frequency, the resulted output signal from the WPD-MEMS scheme has been denoted with the red

color waveform which deotes the output current signal from the model across 1 Ohm resistance. Also, the resulted voltage signal from the suggested model has been obtained as shown with the green color waveform. All the resulted waveforms from the suggested power amplifier model have the same etered frequency. This is an indication of the correct operation of our proposed power amplifier model. Next, the frequency response of the resulted signal from the suggested power amplifier model is obtained in Figure 7.

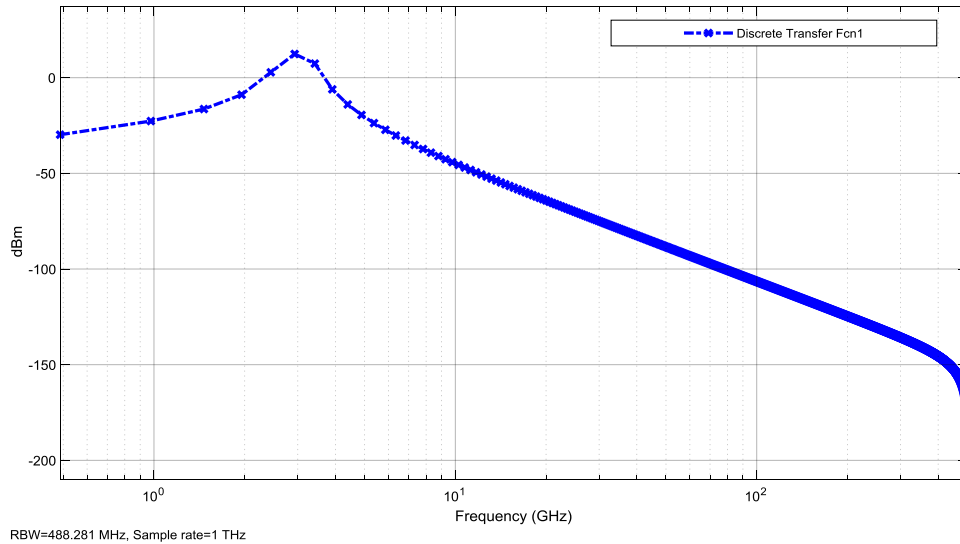


**Figure 7:** The resulted WPD-MEMS frequency response.

Referring to Figure 7, we might observe the chareceristics of the resulted waveform from our suggested WPD-MEMS model, which represeted the frequency response of the sinusoidal resulted waveform at the output of the proposed model. It shows the spectrum of the output wave resulting from a spectral response centered at the filter frequency representative of the operation of the proposed power amplifier. Most of the energy values are concentrated at the working resonant frequency of 3 kHz, while the values of the frequency spectrum decrease as we move away from the effective resonant frequency. Next, the frequency response, or spectrum of the suggested WPD-MEMS model has been achieved as itroduced in Figure 8.

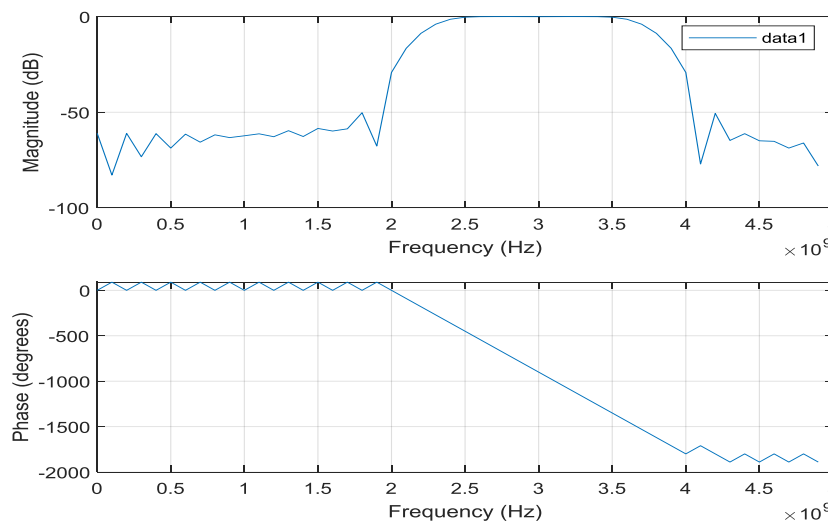


**Figure 8:** Frequency response of the suggested WPD-MEMS model.

By viewing Figure 8, we might observe the spectral magnitude response of the proposed amplifier model which appears as a bandpass filter at a resonant frequency of 3 GHz with a bandpass amplitude of 2 GHz. The figure above also shows the spectral phase response of the proposed amplifier model at the operating resonant frequency of 3 GHz, which is almost a linear response, that indicates the efficiency and reliability of the design.

## 5. CONCLUSIONS

In this study, a Wakinson-type power amplifier was designed based on the properties of ferromagnetic materials (MEMS) and works with high efficiency at ultra-high frequencies for wireless communications to produce cross-band filter characteristics with high-frequency resonator specifications. The characteristics of the amplifier were combined with the specifications of ferromagnetic materials to produce this type of amplifier, which is characterized by its ability to amplify signals up to resonant frequencies of 3 kHz with a pass capacity of up to 2 kHz with an amplification capacity of 90 watts. The proposed model was simulated using Matlab libraries and the proposed amplifier was tested successfully, finding the frequency response to perform its work. The results showed an excellent amplitude response within the designed frequencies, with a linear phase spectrum response operating within the design resonant frequency of 3 kHz with an amplification power of up to 90 watts.

## REFERENCES

1. Feiri, M., Petit, J., and Kargl, F., "The Impact of Security on Cooperative Awareness in VANET," in IEEE Vehicular Networking Conference, VNC, 2014.
2. Asuquo, P., Cruickshank, H., Morley, J., Anyigor Ogah, C.P., Lei, A., Hathal, W., and Bao, S., "Security and Privacy in Location-Based Services for Vehicular and Mobile Communications: An Overview, Challenges and Countermeasures," in IEEE Internet of Things, 2018.
3. Mansour, M. B., Salama, C., Mohamed, H. K., and Hammad, S. A., "CARCLOUD: A Secure Architecture for Vehicular Cloud Computing," in 14th Embedded Security in Cars Europe Conference, ESCAR, Germany, Nov. 2016.
4. Intisar Salem Hamed Al-Mandhari, "A Machine Learning Based Investigation of Cloud Service Attacks", A Doctoral Thesis Submitted in partial fulfillment of the requirements for the award of Doctor of Philosophy of Loughborough University, April 2019. Copyright 2019 Intisar Salem Hamed Al-Mandhari.
5. Rasheed, A., Gillani, S., Ajmal, S., and Qayyum, A., "Vehicular Ad Hoc Network (VANET): A Survey, Challenges, and Applications," in Vehicular Ad-Hoc Networks for Smart Cities, pp. 39-51, Springer, Singapore, 2017. [2] Jaydip Kumar, "Cloud Computing Security Issues and Its Challenges": International Journal of Recent Technology and Engineering (IJRTE) ISSN: 2277-3878, Volume-8, Issue-1S4, June 2019.
6. Wang, S., and Yao, N., "A RSU-aided distributed trust framework for pseudonym-enabled privacy preservation in VANETs," in Wireless Networks, pp.1-17, 2018.
7. Guo, N., Ma, L., and Gao, T., "Independent Mix Zone for Location Privacy in Vehicular Networks," in IEEE Access, 2018.
8. Amro, B., "Protecting Privacy in VANETs Using Mix Zones With Virtual Pseudonym Change," arXiv preprint arXiv:1801.10294, 2018.

9. M. A. Javed, E. Ben Hamida, A. Al-fuqaha, and B. Bhargava, "Adaptive Security for Intelligent Transport System Applications," *IEEE Intell. Transp. Syst. Mag.*, vol. 10, no. April, pp. 110–120, 2018.
10. K. Khanna, B. K. Panigrahi, and A. Joshi, "AI-based approach to identify compromised meters in data integrity attacks on smart grid," 2018.
11. N. Nissim, A. Cohen, and Y. Elovici, "ALDOCX: Detection of Unknown Malicious Microsoft Office Documents Using Designated Active Learning Methods Based on New Structural Feature Extraction Methodology," *IEEE Trans. Inf. Forensics Secur.*, vol. 12, no. 3, pp. 631–646, 2017.
12. H. Sedjelmaci and S. M. Senouci, "An Accurate Security Game for Low-Resource IoT Devices," vol. 66, no. 10, pp. 9381–9393, 2017.
13. Y. Du, J. Wang, and Q. Li, "An android malware detection approach using community structures of weighted function call graphs," *IEEE Access*, vol. 5, pp. 17478–17486, 2017.
14. M. H. Kamarudin, C. Maple, T. Watson, and N. S. Safa, "A LogitBoost-Based Algorithm for Detecting Known and Unknown Web Attacks," *IEEE Access*, vol. 5, pp. 26190–26200, 2017.
15. V. T. Alaparthi and S. D. Morgera, "A Multi-Level Intrusion Detection System for Wireless Sensor Networks Based on Immune Theory," *IEEE Access*, vol. 6, pp. 47364–47373, 2018.
16. M. H. Ali, B. Abbas, D. Al, A. Ismail, and M. F. Zolkipli, "A New Intrusion Detection System Based on Fast Learning Network and Particle Swarm Optimization," *IEEE Access*, vol. 6, pp. 20255–20261, 2018.
17. P. Feng, J. Ma, C. Sun, and Y. Ma, "A Novel Dynamic Android Malware Detection System With Ensemble Learning," *IEEE Access*, vol. 6, pp. 30996–31011, 2018.
18. D. Hu, L. Wang, W. Jiang, and S. Zheng, "A Novel Image Steganography Method via Deep Convolutional Generative Adversarial Networks," *IEEE Access*, vol. 6, pp. 38303–38314, 2018.
19. Y. Gao, Y. U. Liu, Y. Jin, J. Chen, and H. Wu, "A Novel Semi-Supervised Learning Approach for Network Intrusion Detection on Cloud-Based Robotic System," *IEEE Access*, vol. 6, pp. 50927–50938, 2018. [15] G. Tyler, "Information Assurance Tools Report Intrusion Detection Systems," Information Assurance Technology Analysis Center (IATAC), September 2009.
20. C. Yin, Y. Zhu, J. Fei, and X. He, "A Deep Learning Approach for Intrusion Detection Using Recurrent Neural Networks," vol. 5, 2017.
21. N. Shone, T. N. Ngoc, V. D. Phai, and Q. Shi, "A Deep Learning Approach to Network Intrusion Detection," *IEEE Trans. Emerg. Top. Comput. Intell.*, vol. 2, no. 1, pp. 41–50, 2018.
22. H. Peng, Z. Sun, X. Zhao, S. Tan, and Z. Sun, "A Detection Method for Anomaly Flow in Software Defined Network," *IEEE Access*, vol. 6, pp. 27809–27817, 2018.
23. C. Wang, Z. Zhao, L. Gong, L. Zhu, Z. Liu, and X. Cheng, "A Distributed Anomaly Detection System for In-Vehicle Network Using HTM," *IEEE Access*, vol. 6, pp. 9091–9098, 2018.
24. Y. Han, T. Alpcan, J. Chan, C. Leckie, and B. I. P. Rubinstein, "A Game Theoretical Approach to Defend Against Co-Resident Attacks in Cloud Computing : Preventing Co-Residence Using Semi-Supervised Learning," *IEEE Trans. Inf. Forensics Secur.*, vol. 11, no. 3, pp. 556–570, 2016.
25. L. Dritsoula, P. Loiseau, and J. Musacchio, "A Game-Theoretic Analysis of Adversarial Classification," vol. 12, no. 12, pp. 3094–3109, 2017. [17] B. Sevak, "Security against Side Channel Attack in Cloud Computing," *Int. J. Eng. Adv. Technol.*, vol. 2, no. 2, pp. 183–186, 2012.

26. Y Z An, Z F Zaaba, et. al., "Reviews on Security Issues and Challenges in Cloud Computing", International Engineering Research and Innovation Symposium (IRIS) IOP Publishing IOP Conf. Series: Materials Science and Engineering 160 (2016) 012106 doi:10.1088/1757-899X/160/1/012106.
27. Ahmed Khalid Salih, A survey of Cloud Computing Security challenges and solutions", see discussions, stats, and author profiles for this,publicationat:<https://www.researchgate.net/publication/311075805Article>, January 2016
28. Akashdeep Bhardwaj, " Security Algorithms for Cloud Computing", International Conference on Computational Modeling and Security (CMS 2016).
29. Lubna Luxmi Dhirani, et. al., "Tenant - Vendor and Third-Party Agreements for the Cloud: Considerations for Security Provision Article in International Journal of Software Engineering and its Applications · December 2016 DOI: 10.14257/ijseia.2016.10.12.37.
30. Zeinab Lashkaripour," SECURITY IMPLICATIONS AND REQUIREMENTS - CLOUD ENVIRONMENT", Conference Article, July 2016.